

# Dynamic effect of electron-number parity in metal nanoparticles

K. Son<sup>1,2</sup>, D. Park<sup>3,4</sup>, C. Lee<sup>5</sup>, A. Lascialfari<sup>6</sup>, S. H. Yoon<sup>7</sup>, K. -Y. Choi<sup>8</sup>, A. Reyes<sup>9</sup>, J. Oh<sup>10</sup>,  
M. Kim<sup>10</sup>, F. Borsa<sup>6</sup>, G. Schütz<sup>1</sup>, Y. -G. Yoon<sup>5\*</sup>, Z. H. Jang<sup>11\*</sup>

<sup>1</sup>*Department of Modern Magnetic Systems, Max-Planck-Institute for Intelligent Systems, Stuttgart, 70569, Germany.*

<sup>2</sup>*Departement of Physics Education, Kongju National University, Gongju, 32588, Korea.*

<sup>3</sup>*Radwaste Technology Department, Korea Radioactive Waste Agency, Gyeongju 38062, Korea*

<sup>4</sup>*Department of Chemistry, Kookmin University, Seoul 02707, Korea*

<sup>5</sup>*Department of Physics, Chung-Ang University, Seoul 06974, Korea*

<sup>6</sup>*Departimento di Fisica, Università di Pavia, Pavia, Italy*

<sup>7</sup>*Department of Chemistry, Chung-Ang University, Seoul 06974, Korea*

<sup>8</sup>*Department of Physics, Sungkyunkwan University, Suwon 16419, Korea*

<sup>9</sup>*National High magnetic Field Laboratory, Tallahassee, FL 32310, USA*

<sup>10</sup>*Department of Materials Science and Engineering, Seoul National University, Seoul 08826, Korea*

<sup>11</sup>*Department of Physics, Kookmin University, Seoul 02707, Korea*

\* Corresponding authors. Email: [yyoon@cau.ac.kr](mailto:yyoon@cau.ac.kr), [zeehoonj@kookmin.ac.kr](mailto:zeehoonj@kookmin.ac.kr)

Parity is a ubiquitous notion in science and serves as a fundamental principle for describing a physical system. Nanometre-scale metal objects are predicted to show dramatic differences in physical properties depending on the electron-number parity. However, the identification of the electron-number parity effects in real metal nanoparticles has been elusive because of the variations in various features of nanoparticles (size, surface morphology, crystallinity, etc.). Here we report the nuclear magnetic resonance (NMR) detection of the dynamic effect of the electron-number parity in silver nanoparticles. Field and temperature dependences of magnetization are in agreement with the calculations based on the electron-number-parity-dependent model with equal level spacing. With theoretical modeling of the NMR relaxation in silver nanoparticles, the nuclear spin-lattice relaxation rate is found to be proportional to the electron-number-parity-dependent susceptibility and to the temperature. This observation demonstrates the electron-number-parity-governed spin dynamics in silver nanoparticles.

## Introduction

Over the past several decades, tremendous scientific and technological progress has been made in the area of metal nanoparticles research.<sup>1-7</sup> Thanks to their small-size, large surface-to-volume ratio, and discrete energy levels, metal nanoparticles show bizarre physical and chemical properties and hold potential applications in a wide range of fields such as catalysis, magnetic sensing, optical detection, medical diagnosis, etc. Singularly, size, shape, and composition dependence of their properties offer key principles for tailoring and gauging their specific physical or chemical performances and technological functionalities.<sup>2-6</sup> Nevertheless, our knowledge about metal nanoparticles is still limited or incomplete. For example, from the fundamental aspect, our understanding of the physics of the electron-number parity is very limited, even though the electron-number parity is a fundamental attribute that determines the physical properties of metal nanoparticles. The research on this topic can deepen our understanding of the parity effect and open new fields of applications of metal nanoparticles.

Starting in the 1930s, there has been an enormous amount of theoretical studies on the nanometre scale metal structures with unique physical properties.<sup>1,8</sup> Thanks to such efforts, theoretical modeling of nanometre-scale metal nanoparticle as a confined “free” electron system has revealed that thermodynamic properties differ markedly between systems with even and odd number of electrons<sup>9</sup>: in the case of odd parity system, magnetic susceptibility exhibits a Curie-law-like behavior at low temperatures whereas magnetic susceptibility for even parity system vanishes as the temperature is lowered toward zero kelvin (see Fig. 1) Also, alternation of the electron-number parity as a function of field is expected.<sup>9</sup> Since then, several pioneering attempts have been made to detect such parity effects.<sup>10-13</sup> As can be surmised from the rarity of the experimental evidence of the electron-number parity effect, their experimental verification

remains challenging. It is known that the large spin-orbit coupling, non-uniformities in size, non-uniform energy level spacing, etc. can make the electron-number parity effect indistinct.<sup>14, 15</sup> Moreover, a non-uniform distribution of energy level spacing renders the calculation of thermodynamic quantities impractical in many cases. It was not until the mid-1990s that the above-mentioned theoretical predictions were confirmed by measuring the static thermodynamic properties of Pd clusters with a very uniform structure - the number of atoms in the core being the same in all clusters.<sup>16</sup> However, in typical metal nanoparticles, this uniformity is not guaranteed and both types of parity can coexist. The inevitably occurring parity mixing in real nanoparticles disrupts the separation between even- and odd-parity in the static thermodynamic measurements.

Alternatively, from the complete spin pairing in even-parity confinements (all the energy levels are occupied by two electrons with opposite spins) and the existence of the unpaired spins in odd-parity confinements, we infer that the spatiotemporal structure of electron spin correlations can be markedly different between an even- and an odd-parity confinements. (From now on, we will refer to this as the *dynamic electron-number parity effect*.) Therefore, unlike the static thermodynamic quantities, there is a possibility that intermingled dynamic responses of even- and odd-parity confinements can be separated in the time or the frequency domain by utilizing a dynamic probe. The nuclear magnetic resonance (NMR) technique is an excellent experimental tool to probe the dynamical response.

Herein, we report the observation of the dynamic electron-number parity effect in silver nanoparticles (AgNP) synthesized with an archetypical wet chemistry procedure with palmitic acid as the capping agent. <sup>1</sup>H NMR measurements exhibit an unusual double nuclear magnetization relaxation, hinting at two distinct spin correlations. The <sup>1</sup>H NMR nuclear spin-lattice relaxation rates (NSLRs) and the magnetization data are comprehensively analyzed with

electron-number-parity dependent models, giving clear evidence for the existence of both *static* and *dynamic* electron-number parity effect in AgNP. The deduced value of level spacing suggests that the size of the confinement responsible for the electron-number parity effect is smaller than the nominal size of nanoparticles.

## Results

### Static electron-number parity effect

We first examine the magnetization to check the static electron-number parity effect in AgNP specimen. As sketched in Fig. 1b and 1d, the field- and the temperature-dependent magnetization behavior is distinctly different for odd- and even-parity

In spite of the apparent paramagnetic-like behavior of isothermal magnetization (Fig. 2a), simultaneous fitting of the four isothermal  $M_{\text{exp}}(T, H)$ s with the Langevin function could not be done with a common effective magnetic moment, meaning that the magnetism of AgNP is not simple paramagnetism. Instead, we resort to the equal level spacing model by Denton et. al.<sup>9</sup>, which enables the calculation of the magnetization  $m_{\text{odd}}(\delta; T, H)$  [ $m_{\text{even}}(\delta; T, H)$ ] of the confinement with an odd [even] electron-number parity. Here,  $\delta$  is the average value of level spacing of the discrete energy level of AgNP and  $\delta$  is fixed to the value (196.58 K) obtained from the analysis of the NSLR for a consistent analysis of the measured  $M_{\text{exp}}(T, H)$  data and the NSLR data (see Dynamic electron-number parity effect section). Noteworthy is that the average level spacing of  $\delta = 196.58$  K is much larger than the electronic Zeeman energy at the applied magnetic field of  $\mu_0 H_{\text{max}} = 7$  T for our magnetization measurements, thereby the even-parity contribution to  $M_{\text{exp}}(T, H)$  is negligible.<sup>9</sup> Thus, the total magnetization can be approximated as,

$$M_{\text{exp}}(T, H) = N_{\text{odd}} m_{\text{odd}}(\delta; T, H) + \chi_{\text{bg}} H, \quad (1)$$

where  $N_{\text{odd}}$  is the number of the odd parity confinements per gram of AgNP sample and the last term contains the background susceptibility  $\chi_{\text{bg}}$  arising from the capping material, etc. All four isothermal magnetization data were fitted simultaneously and the resultant fitting curves are in good agreement with the experimental data as shown in Fig. 2a. It is deduced from the fitting that  $N_{\text{odd}}$  is  $7.33 \times 10^{18}$  per gram of AgNP and  $\chi_{\text{bg}}$  is  $-1.02 \times 10^{-7} \text{ emu g}^{-1} \text{ Oe}^{-1}$ . The background susceptibility is consistent with that of palmitic acid determined from independent measurement (see Supplementary Information).

Shown in Fig. 2b is the temperature-dependent magnetization measured at  $\mu_0 H_{\text{max}} = 6.55 \text{ T}$ . The temperature-dependent magnetization is compared with the theoretical curve calculated using Eq. (1). In doing that, we used the same parameters obtained from fitting the isothermal  $M_{\text{exp}}(T, H)$ . As such, the coincidence between the theoretical curve and the experimental data gives credence to the employed fitting procedures. The simultaneous description of the field- and temperature-dependent  $M_{\text{exp}}(T, H)$  using the common parameters provides evidence for the existence of the static electron-number parity effect in the AgNP sample.

### **Dynamic electron-number parity effect**

In Fig. 3, we present  $^1\text{H}$  solid-state NMR spectra measured for powder samples of AgNP and capping material (palmitic acid). Almost all the measured spectra exhibit a Gaussian line shape irrespective of temperature and field. Considering its rigid molecular structure and in powder form, the Gaussian spectrum of palmitic acid is reasonable; in fact, for rigid solid with an approximately isotropic angular distribution of inter-nuclear dipolar couplings between protons, the proton NMR line shape is often approximated by a Gaussian function.<sup>17</sup>

On the other hand, there is an additional stronger source of local field at the proton sites of AgNP: the dipolar field of the electron magnetic moments in the AgNP core. The Gaussian spectrum of AgNP implies that the overall static local field at the proton sites has a Gaussian distribution. This is reasonable considering the randomness of the relative orientation/distance between the protons in the capping layer and the electron magnetic moments in the AgNP core.

As can be seen in Fig. 3a and 3b, the centers of the palmitic acid spectra and AgNP spectra coincide with the Larmor frequency of  $^1\text{H}$  NMR without noticeable shift. We also observed that the shifts of the Gaussian lines of the AgNP relative to the spectral lines of the palmitic acid are negligibly small. Thus, we note that the average value of the distribution of the local magnetic field at the proton sites in AgNP due to the electron magnetic moments in the AgNP core is negligibly small.

From Fig. 3, one can also infer that the linewidth of the spectra of palmitic acid and AgNP is temperature and/or field dependent. Investigation on  $^1\text{H}$  solid-state NMR spectra linewidth of palmitic acid and AgNP revealed that the temperature dependence of the linewidth of AgNP is qualitatively explainable in terms of the temperature dependence of the magnetization of the system with odd electron-number parity. Detailed discussion of the temperature dependence and field dependence of the linewidth is given in Supplementary Information.

The nuclear spin-lattice relaxation (NSR) behavior in AgNP shows compelling evidence for the dynamic electron-number-parity effect. Figure 4a exhibits the  $^1\text{H}$  NMR nuclear magnetization recovery curves,  $M(t)$ , of the AgNP and the capping material measured at  $\mu_0 H = 1.299$  T and  $T = 30$  K. Several salient features are found.

First, in contrast to a single stretched-exponential (SE) relaxation behavior observed in the capping material (palmitic acid), we observed a double SE relaxation behavior for AgNP. Since

the proton has a nuclear spin of 1/2, the double SE relaxation is unexpected. The single SE observed in the NSR of the "capping material only" sample indisputably demonstrates that the double SE relaxation of AgNP is definitely due to the influence of the AgNP cores. This observation gives an indication that there are various sources of local field fluctuations at the proton sites of AgNP, i.e., two different types of confinements in the AgNP cores (even- and odd-parity confinements) and capping material itself.

Second, the double SE relaxation gradually turns to a single SE relaxation as the temperature is increased toward  $T = 100$  K as shown in the plot of  $M(t)$  vs.  $\tau T$  in Fig. 4b. ( $\tau$  is the delay between saturation pulse sequence and monitoring pulse sequence.) Figure 4b shows that the slow-relaxing component remains almost the same while the fast-relaxing component gets slower as the temperature is raised.

From the double SE relaxation data of AgNP, two NSLRs are extracted by fitting the  $M(t)$  data with the equation,

$$M(t) = M_0 + M_s[1 - \exp(t/T_{1s}^*)^\beta] + M_f[1 - \exp(t/T_{1f}^*)^\beta], \quad (2)$$

where  $M_0$  is the baseline correction,  $M_s(M_f)$  is the amplitude of the slow(fast)-relaxing component,  $T_{1s}^*(T_{1f}^*)$  is the characteristic relaxation time for the slow(fast)-relaxing component, and  $\beta$  is the common stretching exponent which is fixed to 0.87505 in the fitting. In Fig. 4c and 4d, the resulting NSLRs,  $1/T_{1s}^*$  and  $1/T_{1f}^*$ , are divided by temperature, and plotted as functions of temperature for two different fields. The fast component  $(T_{1f}^*T)^{-1}$  shows a divergent behavior as the temperature is lowered. Above  $T = 100$  K,  $(T_{1f}^*T)^{-1}$  becomes almost temperature-independent and tends to merge with the slow component  $(T_{1s}^*T)^{-1}$ . On the other hand,  $(T_{1s}^*T)^{-1}$  is almost constant in the whole temperature range of measurement. The  $(T_1^*T)^{-1}$  of the capping material measured at 1.299 T is almost independent of temperature and comparable to the slow



component  $(T_{1s}^*T)^{-1}$  (Fig. 4c). This resemblance suggests that the slow component of local field fluctuations mainly arises from the local field fluctuations inherent to the capping material. Thus the very different behavior of the fast component below  $T = 100$  K can be ascribed to the electron-number-parity dependent spin fluctuations in the AgNP core.

Stretched-exponential relaxation occurs when there is a distribution of  $T_1$  and, for a fixed stretching exponent, the value of  $T_1^*$  of a stretched exponential function is usually similar to or scales with the most probable value of  $T_1$  in the distribution.<sup>18</sup> Therefore, from now on, we will use  $T_1$  instead of  $T_1^*$  for simplicity.

The NSLR,  $1/T_1$ , can be expressed as a Fourier transform of the correlation function of the transverse local field fluctuations at the nuclear sites.<sup>19, 20</sup>

$$\frac{1}{T_1} = \frac{\gamma_n^2}{2} \int \langle h_+(t)h_-(0) \rangle e^{i\omega_n t} dt, \quad (3)$$

where  $\langle h_+(t)h_-(0) \rangle$  is the autocorrelation function of the local field fluctuations,  $\omega_n$  is the nuclear Larmor frequency, and  $\gamma_n$  is the nuclear gyromagnetic ratio. The fluctuation of the local field is directly related to the fluctuation of the magnetic moments to which the nuclei are coupled via various interactions. Among them, the dipolar interaction is the dominant one in the investigated sample. Thus, the autocorrelation function of the local field fluctuation is directly related to the correlation function of the magnetic moment fluctuations via dipolar interaction. Our picture of magnetic moments, probing nuclei and coupling between them is schematically sketched in Fig. 5.

The correlation function of the magnetic moment fluctuations can be expressed as a product of the time-independent part and the time-dependent part. The time-independent part can be approximated as a product of the temperature and the static susceptibility.<sup>21, 22</sup> The time-

dependent part is approximated as follows: given that  $^1\text{H}$  NMR of AgNP shows a Gaussian spectrum, it is reasonable to assume that the time dependence of the correlation function is of Gaussian type.<sup>23, 24, 25</sup> As a result, it is deduced that the NSLR,  $1/T_1$ , is proportional to the product of the temperature  $T$  and the magnetic susceptibility  $\chi$  as (see Supplementary Information for detail),

$$1/T_1 \propto T\chi \text{ and } 1/T_1 = \alpha T\chi. \quad (4)$$

We also devised a second model with the concept of spin diffusion in the hydrodynamic limit. In this model, it is assumed that the spin diffusion is restricted inside the nanometre-sized confinement. This second model also revealed that NSLR ( $1/T_1$ ) is proportional to  $T\chi$ , the same as the first model (see Supplementary Information for detail).

The magnetic moments responsible for the local field fluctuations are the electron spin moment in the AgNP cores and the magnetic moments in the background (capping material, etc.). Thus, the autocorrelation function of the local field fluctuation can be decomposed into two parts - one from the AgNP cores and the other from the background. The final equation for fitting the NSLR data is,

$$\frac{1}{T_1 T} = \alpha_{\text{np}} \chi_{\text{np}} + \alpha_{\text{bg}} \chi_{\text{bg}} = \alpha_{\text{np}} \left( \chi_{\text{np}} + \frac{\alpha_{\text{bg}}}{\alpha_{\text{np}}} \chi_{\text{bg}} \right) \equiv \alpha (\chi_{\text{np}} + \eta), \quad (5)$$

where  $T_1$  is the proton spin-lattice relaxation time,  $\chi_{\text{np}}$  is the magnetic susceptibility ( $dM/dH$ ) of the AgNP core, and  $\chi_{\text{bg}}$  represents the average magnetic susceptibility stemming from all other materials in the AgNP specimen.  $\alpha_{\text{np}}$  and  $\alpha_{\text{bg}}$  are the proportionality constants for the AgNP core and the background, respectively. The parameter  $\eta$  is defined as  $\eta = (\alpha_{\text{bg}}/\alpha_{\text{np}})\chi_{\text{bg}}$  which accounts for the background contribution (see Supplementary Information for detail).

With the equal level spacing formalism,<sup>9</sup> we calculate the magnetic susceptibilities  $\chi_{\text{np}} =$

$\chi_{\text{np}}(\delta; T, H)$  for the even- and odd-number parity confinements. The calculated susceptibilities are used in the fitting of the measured NSLR data. By using Eq. (5), we fitted the two sets of  $(T_{1\text{F}}^*T)^{-1}$  data simultaneously with the three common fitting parameters  $(\delta, \alpha, \eta)$  (see Fig. 4c and 4d). The odd-parity susceptibility is used in the fitting since the divergent behavior of  $(T_{1\text{F}}^*T)^{-1}$  is very similar to that of the odd-parity susceptibility. It is reasonable because, in the even-parity cases, spin pairing leads to the cancellation of the magnetic moments. On the other hand, in the odd-parity cases, there is one unpaired electron in each confinement and the fluctuations of the unpaired electron give rise to dominant effects on the nuclear spin-lattice relaxation.

As is evident in Fig. 4c and 4d, the theoretical curves reproduce the experimental data well. The fitting parameters obtained from the fitting are  $\delta = 196.58$  K,  $\alpha = 3.74 \times 10^{25}$  Oe/(s·K·emu), and  $\eta = -6.23 \times 10^{-27}$  emu/Oe. In Fig. 4c and 4d, we plot  $1/T_1T$  vs.  $T$  calculated with the even-parity susceptibility using the same parameters extracted from the odd-parity fitting. The calculated even-parity  $1/T_1T$  lies below the slow component  $(T_{1\text{S}}^*T)^{-1}$ , indicating that the even-parity  $T_1$  is longer than the intrinsic  $T_1$  of the background.

## Discussion

Now we discuss the physical relevance and ramification of the extracted fitting parameters. First, we start with the average energy level spacing  $\delta$  of the discrete energy levels of the AgNP core. In a free electron model, with the bulk electron density of silver, the confinement volume  $V$  and  $\delta$  are related as <sup>1</sup>,

$$V [\text{cm}^3] = 1.45 \times 10^{-18} / \delta [\text{K}]. \quad (6)$$

Using Eq. (6), we find that the energy level spacing of  $\delta = 196.58$  K corresponds to spherical confinement with a diameter of 2.4 nm. This value is several times smaller than the average particle size of 7.31 nm deduced from the SEM image analysis (see Supplementary Information). Rather, it is found to be close to an average domain size of 3.25 nm obtained from XRD analysis (see Supplementary Information). This finding suggests that the confinement of electrons responsible for the electron-number parity effect occurs at the domain level, not throughout the whole particle. Despite the poor crystallinity of the silver core, the shape irregularity, and the difference in the electron density between bulk and nanoparticles, the similarity of the values of the domain size extracted from NMR and XRD is quite remarkable.

We must note that Eq. (6) is based on a free electron model. In reality, the electrons in the AgNP core are not completely free. The very poor crystallinity of the AgNP core puts it in a category of an amorphous material and the electrons in AgNP are confined in the nanometre scale region. Therefore, the physical properties of electrons in the AgNP core will differ from those of bulk crystalline silver or free electrons, and thus, it is highly possible that its  $V$ - $\delta$  relationship deviates from Eq. (6).

The electronic energy level spacing in nanometre-scale confinement is affected by the variations in the physical shape of the confinement, surface structure, irregular crystallinity, etc. As a consequence, an energy level structure varies from confinement to confinement. Thus, in calculating physically observable quantities, the variation should be treated statistically.<sup>1, 9, 26</sup> We also would like to point out that, in our study, we could reproduce the experimental data without such statistical processing. When the temperature is low enough compared to the level spacing between the Fermi level and the first excited state level ( $k_B T < \delta$ ), an equal level spacing scheme is quite a good approximation even without rigorous statistical processing since the populations of higher excited states are negligibly small and, thus, the structure of the higher

excited states is not important. (We stress that the notable changes of the static and dynamical effects are observed at temperatures below 100 K, which lies well below  $\delta = 196.58$  K.)

Now, we proceed with the physical interpretation of  $\alpha$  and  $\eta$ . We could derive the expression of  $\alpha$  by resorting to two different models (or approximations) of the correlation functions mentioned before. With the expression and from the fitted value of  $\alpha$ , the average distance between the protons and the electrons in AgNP is estimated to be  $\sim 2.5$  nm (see Supplementary Information for detail). This value agrees with the morphology of the samples. We further recall that the local field at the  $^1\text{H}$  nuclei sites in AgNP is induced by the magnetic moments in the AgNP. Since the capping material is diamagnetic in nature, its net moment under an external magnetic field is anti-aligned to the electronic moments in the silver core. It results in a diminished effective magnetic field at the proton sites and thus, less fluctuations of the field. This gives a rationale for the negative value of  $\eta$  in Eq. (5).

In summary, we have demonstrated electron-number-parity-dependent spin dynamics with  $^1\text{H}$  NMR spectroscopy in a silver nanoparticle system. We have shown that the NSLRs provide a powerful way to separate odd-parity physics from even-parity physics in nanometre-scale systems such that  $1/T_1T$  is proportional to the parity-dependent susceptibility, allowing the detection of the dynamic electron-number parity effect. Our work opens new horizons for an in-depth understanding of electron-number parity effects in nanoparticles.

## References

1. Halperin WP. Quantum size effects in metal particles. *Reviews of Modern Physics* 1986, **58**(3): 533-606.
2. Braun GB, Friman T, Pang H-B, Pallaoro A, de Mendoza TH, Willmore A-MA, *et al.* Etchable plasmonic nanoparticle probes to image and quantify cellular internalization. *Nature Materials* 2014, **13**(9): 904-911.
3. Boettcher SW, Strandwitz NC, Schierhorn M, Lock N, Lonergan MC, Stucky GD. Tunable electronic interfaces between bulk semiconductors and ligand-stabilized nanoparticle assemblies. *Nature Materials* 2007, **6**(8): 592-596.
4. Yoon B, Luedtke WD, Barnett RN, Gao J, Desireddy A, Conn BE, *et al.* Hydrogen-bonded structure and mechanical chiral response of a silver nanoparticle superlattice. *Nature Materials* 2014, **13**(8): 807-811.
5. Blackman J. *Metallic Nanoparticles*. Elsevier Science, 2008.
6. Thota S, Crans DC. *Metal Nanoparticles: Synthesis and Applications in Pharmaceutical Sciences*. Wiley, 2018.
7. Marbella LE, Millstone JE. NMR Techniques for Noble Metal Nanoparticles. *Chemistry of Materials* 2015, **27**(8): 2721-2739.
8. Fröhlich H. Die spezifische wärme der elektronen kleiner metallteilchen bei tiefen temperaturen. *Physica* 1937, **4**(5): 406-412.
9. Denton R, Mühlischlegel B, Scalapino DJ. Thermodynamic Properties of Electrons in Small Metal Particles. *Physical Review B* 1973, **7**(8): 3589-3607.
10. Yee P, Knight WD. Quantum size effect in copper: NMR in small particles. *Physical Review B* 1975, **11**(9): 3261-3267.
11. Yu I, Halperin WP. The microelectronic structure of platinum particles investigated by NMR. *Journal of Low Temperature Physics* 1981, **45**(1): 189-232.
12. Kimura K, Bandow S, Sako S. Magnetic susceptibilities of small particles of magnesium and beryllium. *Surface Science* 1985, **156**: 883-887.
13. Millet JL, Borel JP. g-factor of magnesium particles of diameter between 10 and 30 Å. *Solid State Communications* 1982, **43**(3): 217-220.
14. Shiba H. Effect of spin-orbit interaction on the Knight shift of normal and superconducting small particles. *Journal of Low Temperature Physics* 1976, **22**(1): 105-119.

15. Sone JI. Effect of Spin-Orbit Interaction on the Spin Susceptibility of Small Particles. *Journal of the Physical Society of Japan* 1977, **42**(5): 1457-1462.
16. Volokitin Y, Sinzig J, de Jongh LJ, Schmid G, Vargaftik MN, Moiseevi II. Quantum-size effects in the thermodynamic properties of metallic nanoparticles. *Nature* 1996, **384**(6610): 621-623.
17. MacKay AL. A proton NMR moment study of the gel and liquid-crystalline phases of dipalmitoyl phosphatidylcholine. *Biophysical Journal* 1981, **35**(2): 301-313.
18. Johnston DC. Stretched exponential relaxation arising from a continuous sum of exponential decays. *Physical Review B* 2006, **74**(18): 184430.
19. Abragam A. *The Principles of Nuclear Magnetism*. Clarendon Press, 1961.
20. Carretta P, Lascialfari A. *NMR-MRI,  $\mu$ SR and Mössbauer Spectroscopies in Molecular Magnets*. Springer Milan, 2007.
21. Dolinšek J, Vilfan M, Žumer S. *Novel NMR and EPR Techniques*. Springer Berlin Heidelberg, 2009.
22. Moriya T. Nuclear Magnetic Relaxation near the Curie Temperature. *Progress of Theoretical Physics* 1962, **28**(2): 371-400.
23. Anderson PW, Weiss PR. Exchange Narrowing in Paramagnetic Resonance. *Reviews of Modern Physics* 1953, **25**(1): 269-276.
24. Moriya T. Nuclear Magnetic Relaxation in Antiferromagnetics, II. *Progress of Theoretical Physics* 1956, **16**(6): 641-657.
25. Gulley JE, Hone D, Scalapino DJ, Silbernagel BG. Exchange Narrowing: Magnetic Resonance Line Shapes and Spin Correlations in Paramagnetic  $\text{KMnF}_3$ ,  $\text{RbMnF}_3$ , and  $\text{MnF}_2$ . *Physical Review B* 1970, **1**(3): 1020-1030.
26. Kawabata A. Electronic Properties of Fine Metallic Particles. III. E.S.R Absorption Line Shape. *Journal of the Physical Society of Japan* 1970, **29**(4): 902-911.

## **Acknowledgments**

### **Author contributions**

K. S. and G. S. performed SQUID measurement. K. S. and Z. H. J. carried out magnetization analysis. K. S. and G. S. performed XPS characterization. D. P. and S. H. Y. performed material synthesis and preliminary characterization (TEM, SEM, ICP-AES, TGA, XRD). J. O. and M. K. performed HRTEM measurement. C. L., K. Y. C., A. R., and Z. H. J. performed NMR experiment. A. L., F. B., Y.-G. Y. and Z. H. J. carried out analysis of the NMR data. A. L., F. B., Y.-G. Y., and Z. H. J. developed theoretical interpretation of the results. All authors discussed the results and participated in writing manuscript, and commented on the manuscript.

### **Competing interests**

Authors declare no competing interests.



## **Additional information**

**Supplementary Information** is available for this paper

**Correspondence and requests for materials** should be addressed to Z. H. J.

## Methods

### Synthesis

The Ag nanoparticles (AgNP) were synthesized by modifying the method reported in the literature.<sup>27</sup> AgNO<sub>3</sub> (purity > 99.5 %), toluene (purity > 99.5 %), trimethylamine (purity = 98 %), and palmitic acid were purchased from Sigma-Aldrich and used as received. Briefly, palmitic acid (5.6 g) was dissolved in triethylamine (40 mL) followed by the addition of AgNO<sub>3</sub> (3.6 g). After 10 min stirring, the solution changed to white slurry which was refluxed at 80 °C for 2 h. The synthesized Ag nanoparticles were purified three times by addition of acetone (35 mL) followed by centrifugation at 4000 rpm for 10 min. The as-synthesized Ag nanoparticles were dispersed in hexane (0.5 wt %, brown).

### Morphology and crystallinity characterization

**TEM/SEM** Samples for Transmission Electron Microscope (TEM) analysis were prepared by dropping Ag nanoparticles dispersed in hexane (0.5 wt %) on an amorphous carbon-coated copper grid. The images were obtained with JEOL JEM-2100F (200 keV). High-Resolution TEM observations were conducted using a Cs-corrected TEM operated at 300 kV (Themis Z S/TEM, Thermo Fisher Scientific). To take the Scanning Electron Microscope (SEM) images of the Ag nanoparticles, the particles were mounted on specimen stubs with double-sided adhesive carbon tape and coated with Au in a sputter coater for 2 min to avoid charging. SEM images were obtained with Hitachi FE-SEM S-4800.

**X-ray Diffraction** The X-ray diffraction pattern of the Ag nanoparticles was obtained with X-ray diffractometer (XRD; Bruker D8 Focus) using Cu K $\alpha$  radiation.

## **Impurity and Composition characterization**

**TGA** Thermal Gravimetric Analysis (TGA) was performed with TA instruments STA-1500 to quantitatively determine the amounts of the capping material. The heating rate was 10 °C/min and the analysis was performed under N<sub>2</sub> atmosphere.

**ICP-AES** The Inductively Coupled Plasma (ICP)-Atomic Emission Spectrometry (AES) measurements were performed with thermo elemental iris intrepid ICP-AES spectrometer system. Samples for ICP-AES analysis were prepared by dissolving Ag nanoparticles (0.200 g) in nitric acid (10 mL).

**XPS** The X-ray Photoemission Spectroscopy (XPS) was performed to analyse elemental composition and to check impurity with Thermo VG Theta Probe system (Thermo Fisher Scientific, USA.) The system employs monochromatic Al K $\alpha$  radiation ( $h\nu = 1486.68$  eV) produced with an electrical power of 100 W. The base pressure was  $8 \times 10^{-8}$  mbar. The X-ray spot size was about 400  $\mu\text{m}$  in diameter.

## **Magnetic property characterization**

The magnetic properties of the silver nanoparticles (AgNP) were investigated using a commercial superconducting quantum interference magnetometer (SQUID, Quantum Design MPMS-XL, USA). Field-dependent magnetization was measured at various temperatures by varying the field in the range  $0 \leq T \leq 7$  T. Temperature-dependent magnetization was investigated at 6.55 T. Since overall signal of the sample is not significantly large, extra care has been exercised during the preparation and the measurement process to avoid sample

contamination, e. g. all the metallic tools were excluded in the sample preparation procedures not to contaminate sample with the magnetic impurities.

### **Solid-state nuclear magnetic resonance (NMR) experiment**

$^1\text{H}$  NMR was performed at NHMFL at Tallahassee, FL. U.S.A. utilizing user facility (wide band solid-state NMR - 12 T sweepable superconducting magnet, home-made VTI (Variable Temperature Insert) and in-house developed pulsed RF FFT NMR spectrometer).

**$^1\text{H}$  NMR spectrum** Spectra of AgNP and capping material were obtained by performing FFT (Fast Fourier Transform) on half of the Hahn echo. The length of  $\pi/2$  pulse was in the range from 1.15 to 7 microseconds. The spectral width of RF pulses is confirmed to be always larger than the linewidth of the AgNP spectra.

**$^1\text{H}$  NMR spin-spin relaxation ( $T_2$ )** Spin-spin relaxation time  $T_2$ 's of AgNP and capping material were measured as functions of temperature at 1.299 T (both AgNP and capping material) and 3.0 T (AgNP only) with the conventional Hahn echo sequence ( $\pi/2 - \pi$ ). The relative phase between the first and the second pulses has been varied according to the 16 phase cycling scheme to reduce the distortion due to the ringing.<sup>28</sup>  $\pi/2$  pulse length ranged from 1.15 to 7 microseconds and single exponential relaxation behavior was observed in all the measurements of the AgNP and the capping material (palmitic acid).

**$^1\text{H}$  NMR nuclear spin-lattice relaxation ( $T_1$ )**  $^1\text{H}$  NMR nuclear spin-lattice relaxation ( $T_1$ ) behavior was investigated at two fields (1.299 T and 3.0 T) as functions of temperature. The saturation recovery sequence was utilized in all the measurements with ( $\pi/2$ ) pulse length

ranging from 1.15 to 7 microseconds depending on the tuning and matching conditions of the RF probe system. Nuclear magnetization recovery data were obtained by recording echo height as functions of delay between the saturation pulse sequence and the monitoring pulse sequence. Saturation pulse sequence is composed of one or two ( $\pi/2$ ) pulses of which the separation is longer than  $T_2$  and much shorter than  $T_1$  measured at the same field and temperature conditions.

## References

27. Yamamoto M, Nakamoto M. Novel preparation of monodispersed silver nanoparticles via amine adducts derived from insoluble silver myristate in tertiary alkylamine. *Journal of Materials Chemistry* 2003, **13**(9): 2064-2065.
28. Claridge TDW. *High-Resolution NMR Techniques in Organic Chemistry*. Elsevier: Boston, 2016.

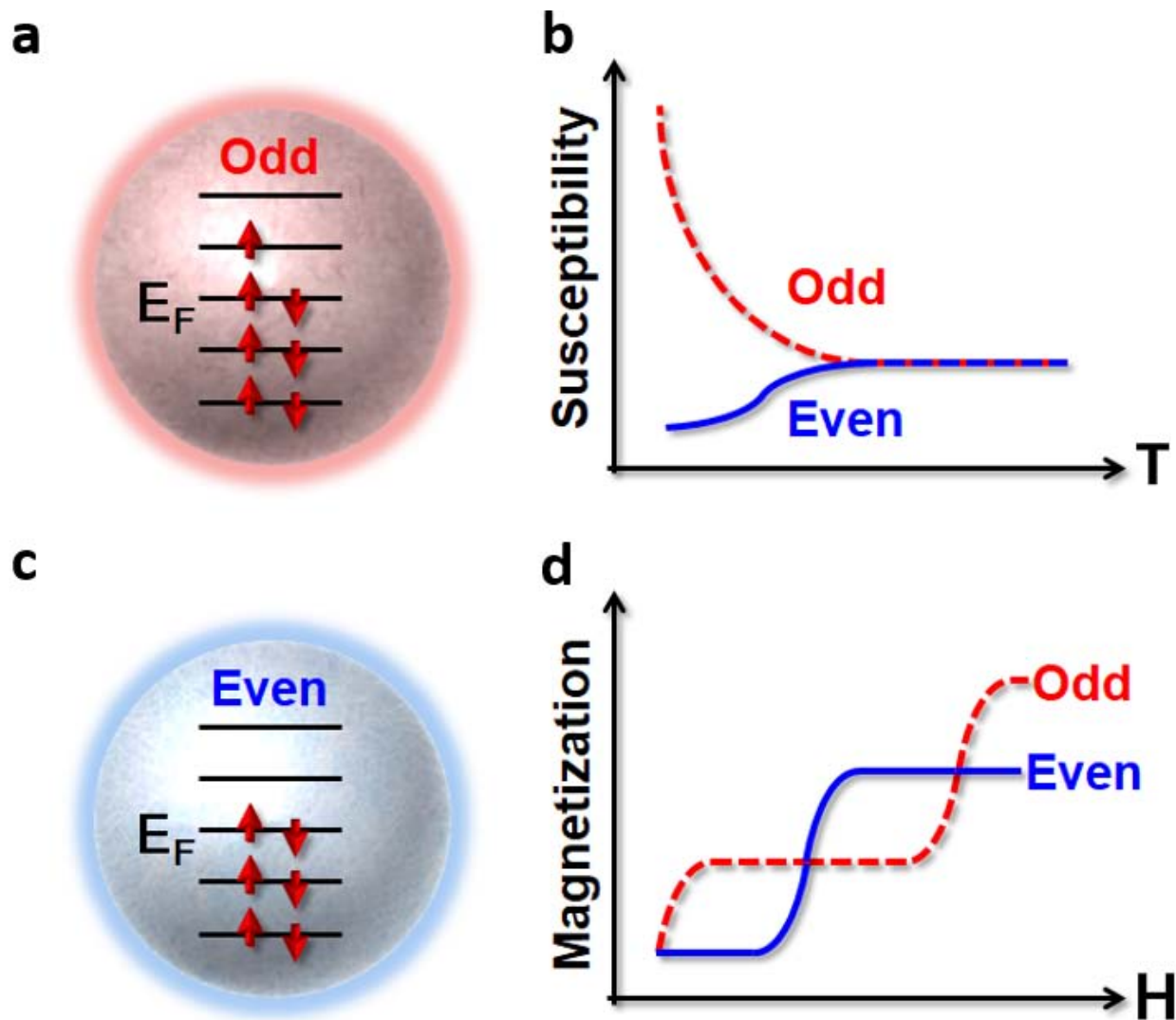


**Fig. 1. Schematic sketch of electron-number parity dependent magnetization and magnetic susceptibility.** **a, c**, Ground state electronic configurations. If an odd number of electrons are confined together (odd number parity, **a**), discrete energy levels up to the Fermi level are filled with two electrons (spin up and spin down pair) and the level just above the Fermi level is occupied by one unpaired electron. A divergent behavior of the temperature-dependent magnetic susceptibility (red dashed line in **b**) and a steep initial increase followed by a plateau in the field-dependent magnetization (red dashed line in **d**) originate from the unpaired electrons. If an even number of electrons are confined together (even number parity, **c**), all the energy levels up to the Fermi level are filled with two electrons and all the electrons are paired. The suppression of a temperature-dependent susceptibility (blue line in **b**) and an almost field-independent magnetization plateau at low field (blue line in **d**) result from the paired electron spins. It is worthwhile to note that the field-dependent magnetization alternates between odd- and even-parity behaviors at specific fields (spin-flip transition) whose field strength corresponds to half of the level spacing.<sup>1,9</sup> Similar effect occurs in the field-dependent magnetic susceptibility.

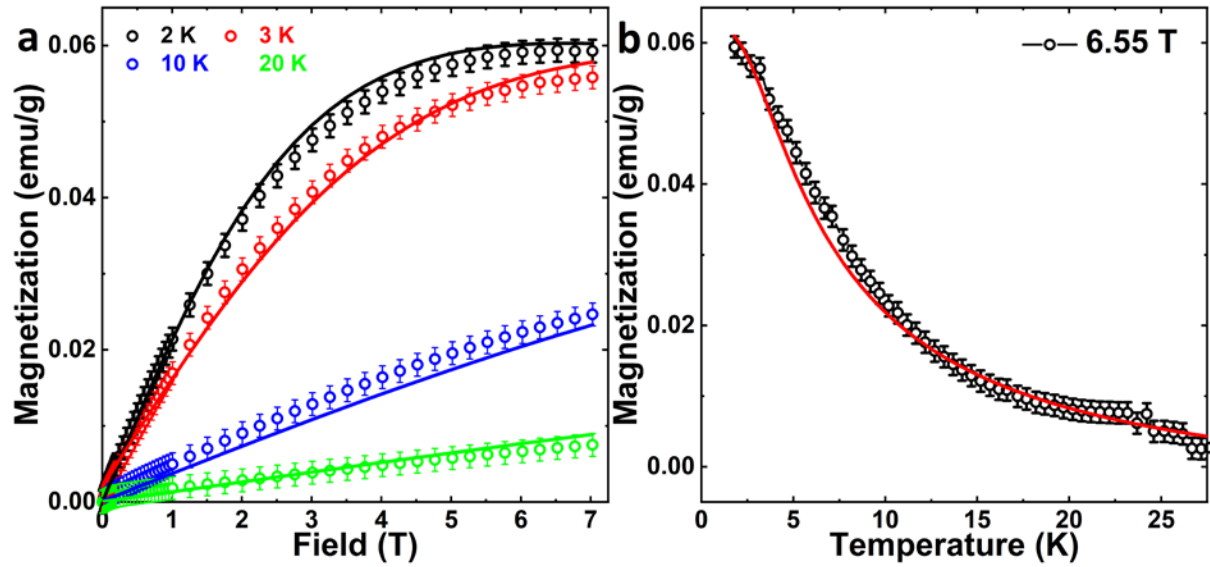


**Fig. 2. Electron-number parity effect in magnetization.** **a**, Isothermal field-dependent magnetization curves measured at four different temperatures ( $T = 2, 3, 10, 20$  K). All the data are in agreement with the theoretical curves (solid lines) calculated with the model described in the main text. **b**, Temperature-dependent magnetization measured at 6.55 T. The red solid line represents the theoretical curve calculated using the same parameters deduced from the field-dependent isothermal magnetization fitting. The good agreement between the experimental and calculated magnetization provides independent confirmation of the model adopted in the analysis.

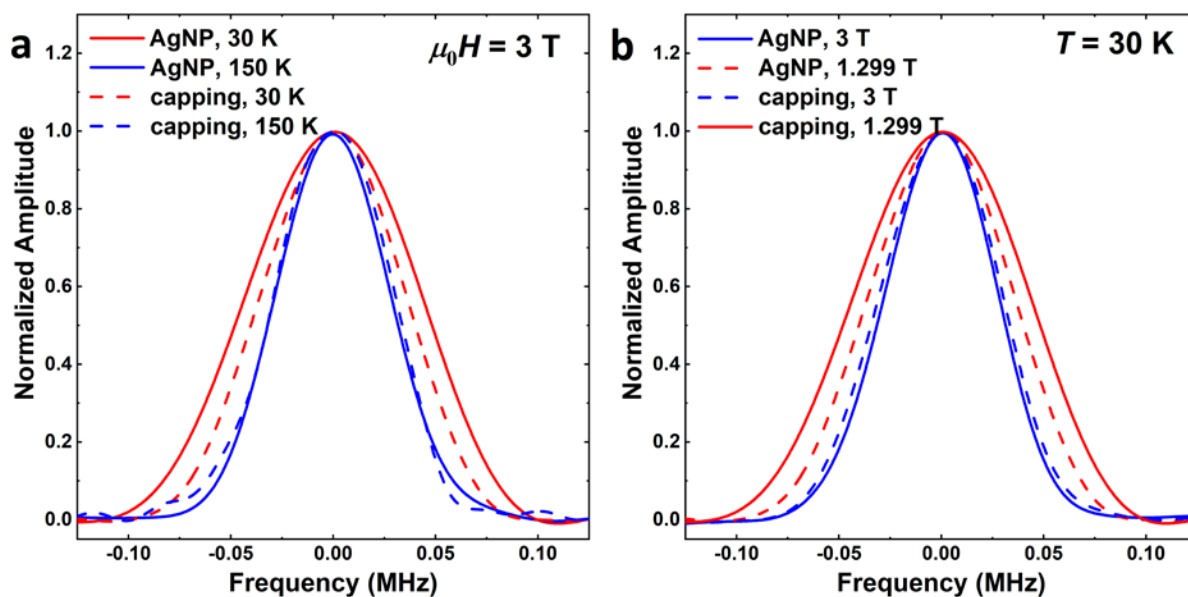


**Fig. 3.  $^1\text{H}$  NMR spectra of silver nanoparticle.** **a**, Temperature dependent  $^1\text{H}$  NMR spectra of the AgNP and palmitic acid measured at 3.0 T, showing a Gaussian spectral shape and the increase of linewidth (FWHM) as the temperature is lowered. It is shown that the linewidth and shape of the spectra of the AgNP and palmitic acid are very similar to each other at high temperatures. **b**, Field dependent spectra of the AgNP and palmitic acid measured at 30 K. The spectral shape (Gaussian) is independent of the field, but the linewidth (FWHM) of the 3.0 T spectrum is larger than that of the 1.299 T spectrum, showing that the linewidth is field dependent. The spectra of palmitic acid from the separate measurements are also shown for comparison. It is noted that the scales of x-axis are expressed relative to the  $^1\text{H}$  Larmor frequency in both graphs.



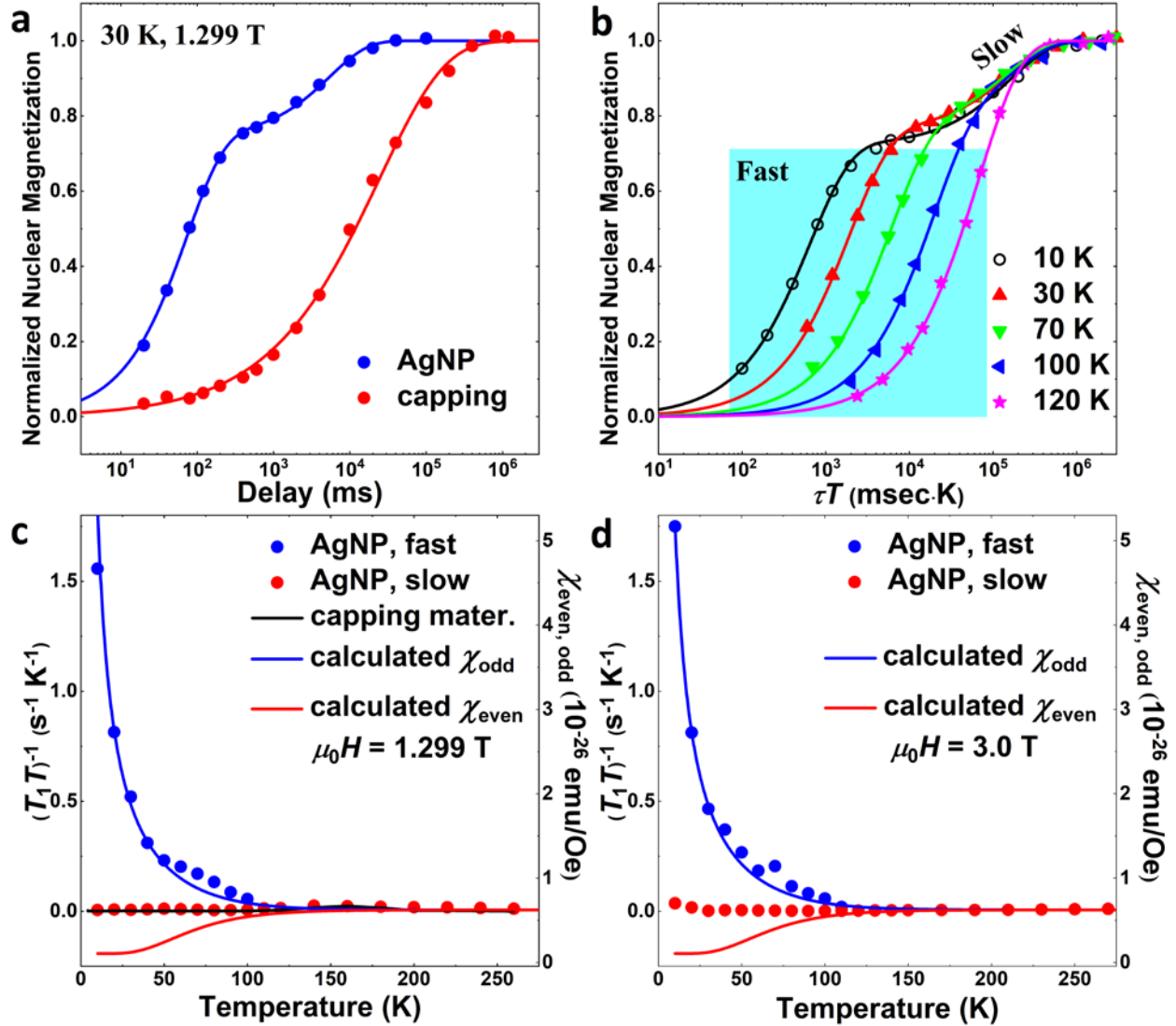


**Fig. 4. Electron-number parity dependent spin dynamics measured by nuclear spin-lattice relaxation of  $^1\text{H}$  NMR.** **a**,  $^1\text{H}$  NMR nuclear magnetization recovery curves of AgNP and capping material measured at  $\mu_0 H = 1.299$  T and  $T = 30$  K. Solid lines are fits to single stretched-exponential (capping material) and double stretched-exponential (AgNP). A double-step structure in the recovery of AgNP corroborates double stretched-exponential relaxation which is in contrast to the single stretched-exponential relaxation of the capping material. **b**,  $^1\text{H}$  nuclear magnetization versus  $\tau T$  clearly shows that the fast component  $1/T_1 T$  is strongly temperature-dependent. In contrast, the slow-component varies little with temperature. **c**, **d**,  $1/T_1 T$  vs.  $T$  of AgNP and capping material measured at 1.299 T and 3.0 T. For both fields, the fast component  $1/T_1 T$  (blue circles) is divergent as the temperature is lowered below 100 K and almost constant above 100 K. The behavior is reminiscent of the odd parity susceptibility.<sup>9</sup> The slow component  $1/T_1 T$  (red circles) and the  $1/T_1 T$  of capping material (black solid line) are almost constant and coincide with each other over a whole temperature range (see **c**), suggesting that the slow component spin dynamics is dominated by the local field fluctuations inherent to capping material. The fast component  $1/T_1 T$  data are successfully fitted with Eq. (5) using the electron-number-parity dependent susceptibility obtained from the equal level spacing model<sup>9</sup> (see blue solid lines.)

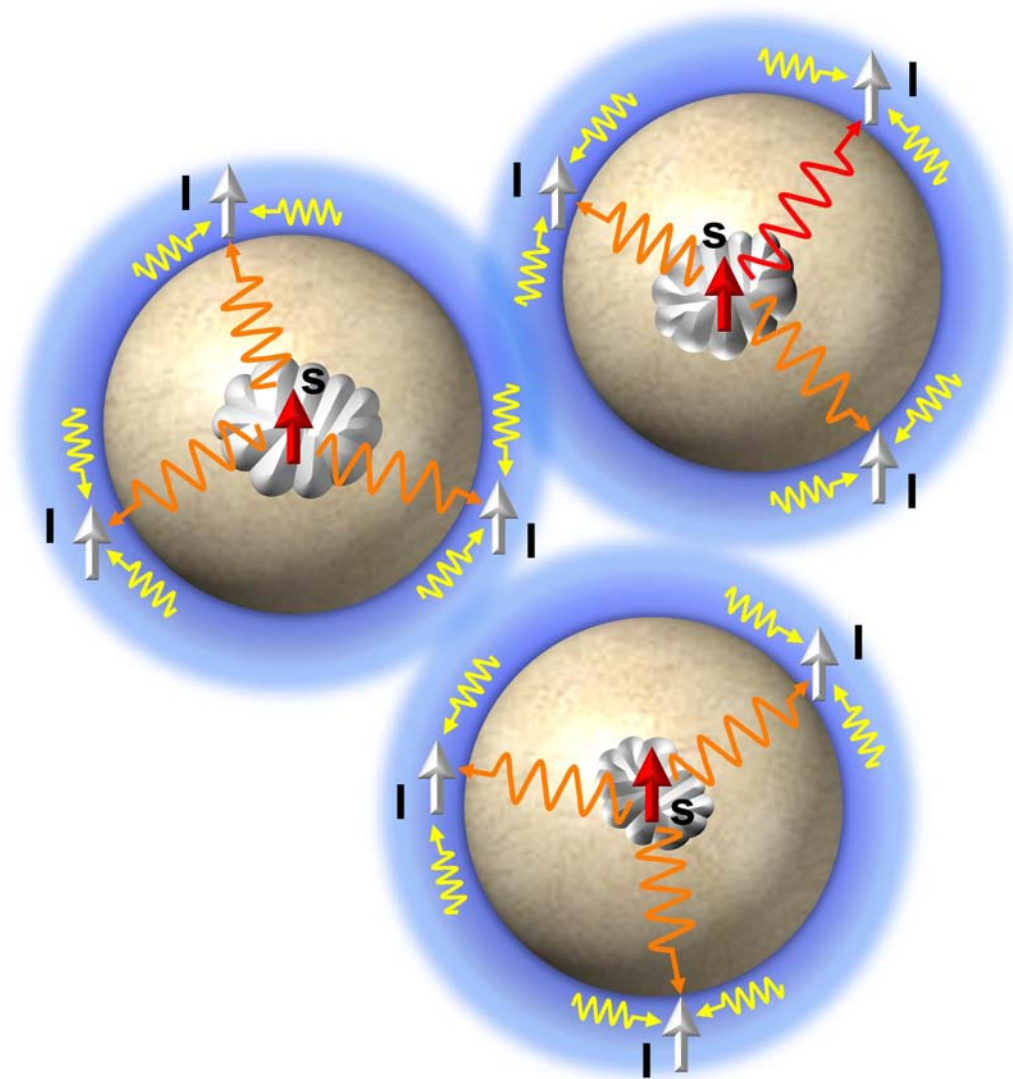


**Fig. 5. Schematic view of NMR detection of the spin dynamics in AgNP.** The unpaired electronic spins ( $s$ ) in the silver cores are indicated by red arrows. Peach colored areas represent the silver core and shaded gray areas denote domains with odd electron-number parity. The blue circular ring regions are the capping material of AgNP. Light gray arrows are  $^1\text{H}$  nuclei ( $I$ ) existing in the capping material. The local field at  $^1\text{H}$  nuclei ( $I$ ) is composed of a dipolar field (orange wavy line) arising from the electron spins in the silver core and a dipolar field (yellow wavy line) arising from moments in the capping material.